CFD ANALYSIS OF THE EFFECT OF HETEROGENEOUS HULL ROUGHNESS ON SHIP RESISTANCE

Roberto RAVENNA[1], Soonseok SONG, Weichao SHI, Tonio SANT, Claire DE MARCO MUSCAT-FENECH, Yigit Kemal DEMIREL

ABSTRACT

Hull roughness increases ship resistance, power, and fuel consumption significantly. Recent studies have demonstrated that Computational Fluid Dynamics (CFD) can accurately predict the effect of roughness on ship resistance by using a modified wall-function approach. Although hull roughness is often spatially heterogeneous, little research has been carried out on the heterogeneous roughness effect on ship resistance.

Therefore, this study aims to investigate the heterogeneous roughness effect on ship resistance using CFD. A series of CFD simulations were conducted on a scaled model of the KRISO Container Ship (KSC) hull. Various surface coverage conditions were considered, including homogeneous (i.e., smooth, and full-rough conditions) and heterogeneous conditions (i.e., different smooth/rough wetted surface ratios).

The present findings showed that increased roughness on the fore hull regions has a greater impact on ship resistance than the rough aft-hull regions. The introduction of a so-called roughness impact factor correlated the added resistance of the heterogeneous roughness scenarios to the corresponding rough wetted surface area. Accordingly, the rough fore-hull scenarios presented higher roughness impact factors than the rough aft-hull cases.

Keywords: Roughness Effect; Heterogeneous Roughness; Ship Resistance; Computational Fluid Dynamics (CFD); KRISO Container Ship (KCS).

1. Introduction

It is well established that hull roughness is foremost responsible for the decay of ship performance over time. Biofouling accumulation, coatings failure and corrosion are the leading causes of the increase of roughness on the hull surfaces [1], [2]. Naval architects, shipowners, and operators are fully aware of the economic and environmental penalties linked to a poorly maintained hull. Nevertheless, our understanding of the hull roughness effect on ship resistance is still limited. Dry-dock and fouling control coating (FCC) strategies to mitigate the roughness effect on ship resistance are arguably incomplete. The approach of ignoring the vessel's underwater hull conditions for long dry-dock intervals leads to considerable losses on a fleet's economy.

Theoretical and numerical methods based on the turbulent boundary layer theory can accurately predict the roughness effect on ship resistance, provided that the roughness function of the surface is known [3]. Researchers, e.g., [4]–[10], have widely adopted Granville's similarity law scaling procedure, [11], [12], due to its robustness and cost-effectiveness [13]. However, Granville's theoretical method is limited by a number of simplifications. In fact, the 2D flat plate assumption neglects the 3D effect [14], and the assumption of a constant roughness function along the flat plate may lead to scaling problems and inaccurate added resistance predictions [15].

An alternative to Granville's method is Computational Fluid Dynamics (CFD), which is cost-efficient compared to experimental approaches and can overcome related shortcomings [14]. The CFD approach avoids the nonlinear problems of theoretical studies and dynamically computes the roughness function for each discretised cell [16]–[18]. Furthermore, the ship resistance predictions are more accurate in CFD since the 3D effect of the hull are considered, and the ship can be modelled in full-scale. Accordingly, several studies recently adopted the CFD approach for investigating the roughness effect on ship resistance, [19]–[21]. Nonetheless, despite the hull roughness distribution of in-service ships is inherently heterogeneous, most published studies have treated the hull roughness as homogeneous.

Recently, Song et al., [22], [23], investigated the heterogeneous hull roughness effect on ship hydrodynamics by means of experimental fluid dynamics (EFD) and CFD. In our previous study, [22], the Wigley hull was modelled with different hull roughness conditions by applying sand-grit on the hull surface in different configurations (i.e.,

1 University of Strathclyde, Department of Naval Architecture, Ocean and Marine Engineering, Faculty of Engineering, Tel: +39 333 3005015, +44 7506 855 938, e-mail: roberto.ravenna@strath.ac.uk

smooth and full- rough, ¼-bow-rough, ¼-aft-rough, ½-bow-rough and ½-aft-rough). In [23], Song et al. performed CFD simulations using the modified wall-function approach and the roughness function model of [18]. In [18] the CFD model was validated to predict the effect of roughness on ship resistance for 3D hulls. The findings showed good agreement between the CFD modified wall-function approach, Granville's similarity law and measurements from towing tests of a ship model test with a rough surface [24]. These studies showed that the increased hull roughness in the forward wetted area of the hull causes further added resistance than the hull roughness in other parts. The findings suggest the possibility of prioritising a partial hull cleaning depending on the impact of the roughness in different hull regions.

Vargas et al. [25] conducted CFD simulations on a surface combatant exposed to different roughness scenarios. The effects of heterogeneous distribution of roughness and the benefits of partial hull cleaning were investigated dividing the hull into sections. The findings indicated that the increase in the skin friction resulting from localised roughness is highest at the bow, followed by sides, flat bottom, stern, and transom. Östman et al. [26] carried out a CFD analysis investigating the potential of a selective application of different quality coatings on a full-scale tanker. Only the regions where high skin friction is concentrated were modelled with high-quality coating (low roughness), while the rest of the hull was modelled with a low-quality coating. The results confirmed the expectations: this selective approach can reduce the ship resistance compared to when the inferior coating is applied on the entire hull.

The promising findings of the few studies addressing the effect of heterogeneous distribution of hull roughness are limited to the ship types considered (the Wigley hull, a tanker, and a surface combatant). Despite these recent studies, our understanding on the effect of heterogeneous hull roughness is still limited. The different impacts of hull roughness according to the different hull regions need to be investigated for better comprehension. The present study aims to fill this research gap by investigating the effect of heterogeneous roughness on the hydrodynamic resistance of the well-known Kriso Container Ship (KCS) hull using CFD, and supporting a targeted strategy for hull maintenance. Furthermore, the CFD simulations provide complete and accurate data to assess how the heterogeneous hull roughness affects the flow regime around the hull.

The present study is a CFD investigation conducted on the benchmark KCS hull in heterogeneous coverage conditions, namely: *Bulbous Bow*, *Fore Hull*, *Midship*, *Flat Bottom*, *Aft Hull,* and *Stern*. The paper is structured as follows: the methodology is explained in Section 2, including the approach and numerical modelling. Details of the modified wall-function approach, mathematical formulations, geometry and boundary conditions, and mesh generations are given in this section. In Section 3 are presented the results of the current CFD investigation. The effects of the heterogeneous roughness on the hydrodynamics of the ship were assessed. The various hull roughness conditions were correlated with the predicted resistance coefficients, roughness Reynolds number values, and boundary layer distributions and the findings compared with the homogeneous full rough and full smooth cases. The conclusions in Section 4 summarise and discuss the findings and suggest recommendations for future studies.

2. Methodology

2.1. Approach

Figure 1 shows a schematic illustration of the CFD methodology adopted to investigate the effect of heterogeneous distributions of hull roughness on the well-known KRISO Container Ship (KCS), [27]. The model-scale numerical towing tests investigated the effect of various heterogeneous hull roughness conditions (different smooth/rough wetted surface coverage ratios) and effects on ship resistance. These roughness scenarios were designed with the aim of investigating the potential of low-cost targeted hull maintenance.

The simulations were developed in the StarCCM+ software package (Version 15.06.007-R8), adopting the Unsteady Reynolds Averaged Navier–Stokes (URANS)-based CFD with the modified wall-function model recently validated by Song et al. [18].

Finally, the skin friction coefficients, C_F, the roughness Reynolds number, k^+, and the boundary layer on the hull surfaces were examined and correlated with the findings. The report figures for these parameters will support a better comprehension of the impact of the increased roughness of different hull conditions on ship resistance.

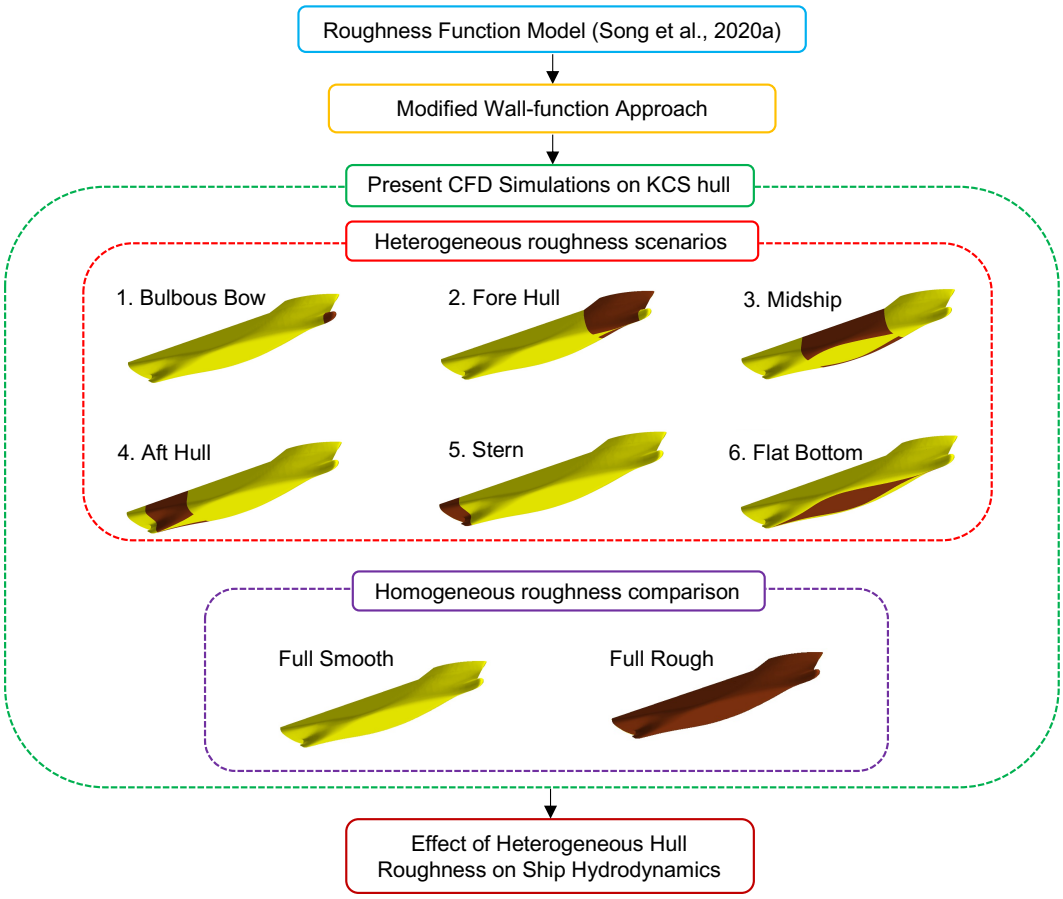

Figure 1. Schematic illustration of the methodology adopted.

2.2. Numerical modelling

2.2.1. Mathematical Formulations

The governing equations of this hydrodynamics study are given in tensor notation and Cartesian coordinates by equation (1) and (2), [28]:

$$\frac{\partial(\rho\bar{u}_i)}{\partial x_i} = 0 \tag{1}$$

$$\frac{\partial(\rho\bar{u}_i)}{\partial t} + \frac{\partial}{\partial x_j}\left(\rho\bar{u}_i\bar{u}_j + \rho\overline{u_i'u_j'}\right) = -\frac{\partial\bar{p}}{\partial x_i} + \frac{\partial\bar{\tau}_{ij}}{\partial x_j} \tag{2}$$

where, ρ is the density, $\bar{u}_i$ is the averaged velocity vector, $\rho\overline{u_i'u_j'}$ is the Reynolds stress, $\bar{p}$ is the averaged pressure, $\bar{\tau}_{ij}$ is the mean viscous stress tensor components. Newtonian fluid's viscous stress can be expressed as in equation (3):

$$\bar{\tau}_{ij} = \mu\left(\frac{\partial\bar{u}_i}{\partial x_j} + \frac{\partial\bar{u}_j}{\partial x_i}\right) \tag{3}$$

where, μ is the dynamic viscosity. Using the Boussinesq hypothesis, the Reynolds stress can be written as in equation (4):

$$-\rho\overline{u_i'u_j'} = \mu_t\left(\frac{\partial\bar{u}_i}{\partial x_j} + \frac{\partial\bar{u}_j}{\partial x_i}\right) - \frac{2}{3}\left(\rho k + \mu_t\frac{\partial\bar{u}_k}{\partial x_k}\right)\delta_{ij} \tag{4}$$

where, μ_t is the turbulent eddy viscosity, k is turbulent kinetic energy, and δ_{ij} is the Kronecker delta.

The above averaged continuity and momentum equations for incompressible flows were solved by the commercial CFD software STAR-CCM+ using URANS and finite volume methods. The CFD solver used a second order upwind convection scheme and a first order temporal discretisation for the momentum equations. On the other hand, the

continuity equations were solved in a segregated manner and linked to the momentum equations with a predictor-corrector algorithm. The k-ω SST (Shear Stress Transport) turbulence model [29] was used with a second-order convection scheme. This turbulent model combines k-ω and k-ε formulations for an accurate near wall treatment of the effects of turbulence, and an overall enhanced prediction in adverse pressure gradients and separating flow. The free surface effects were modelled with the Volume of Fluid (VOF) using High Resolution Interface Capturing (HRIC).

2.2.2. Modified Wall-Function Approach

An increase in surface roughness reduces the boundary layer thickness and causes an increase in flow turbulence. Hence, the turbulent stress, wall shear stress and ultimately the skin friction increase. The roughness effect can also be seen as a downward shift of the non-dimensional velocity profile in the turbulent boundary layer log-law region. The non-dimensional velocity profile (U^+) in the log-law region for a rough surface can be written as equation (5):

$$U^+ = \frac{1}{\kappa}\ln y^+ + B - \Delta U^+ \tag{5}$$

where κ is the von-Karman constant, y^+ is the non-dimensional normal distance from the boundary, ($y^+ = yU_\tau/\nu$), B is the smooth wall log-law intercept. The downward shift of the non-dimensional velocity profile (ΔU^+), also known as "roughness function", is a unique characteristic of a rough surface. In other words, different rough surfaces are characterised by different roughness functions to be modelled experimentally [12]. The roughness function model of the surface can then be implemented in the wall-function of the CFD model. The roughness function, ΔU^+ is a function of the roughness Reynolds number, k^+, which is defined as (6):

$$k^+ = \frac{kU_\tau}{\nu} \tag{6}$$

in which, k is the roughness height of the surface, and U_τ is the velocity based on wall shear stress defined as (7):

$$U_\tau = \sqrt{\tau_w/\rho} \tag{7}$$

where τ_w is the wall shear stress and ρ is the water density.

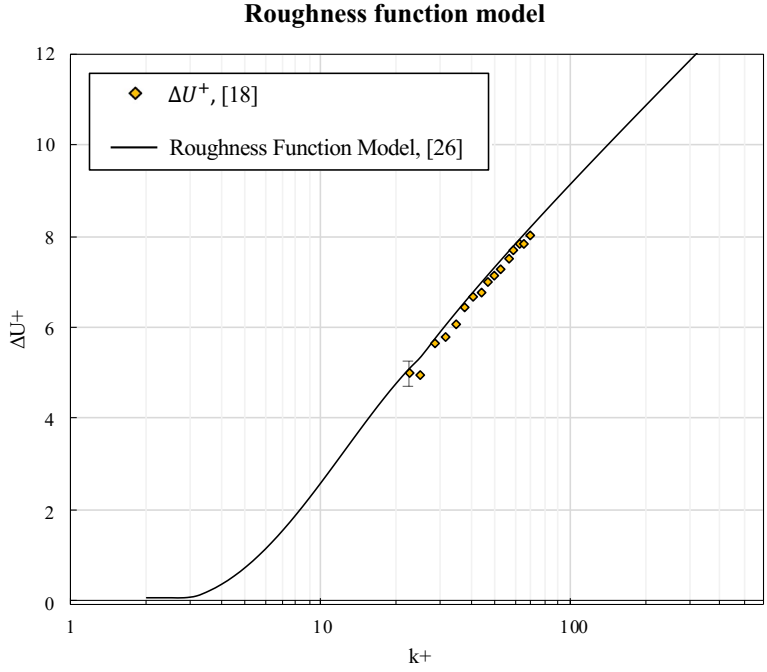

Figure 2. Experimental roughness function of Song et al. [18] and the roughness function model adopted in this study [24].

Figure 2 and equation (8) show the roughness function model employed in this study. Song et al. [18] developed this model from the towing tests of a flat plate covered with sand (aluminium oxide, 60/80 grit) [24]. One may notice that this is a very rough case (roughness height over a 50 mm interval was $k = Rt_{50} = 353$ μm).

$$\Delta U^+ = \begin{cases} 0 & \rightarrow \quad k^+ < 3 \\ \frac{1}{\kappa}\ln\left[0.49k^+ - 3\left(\frac{k^+ - 3}{25 - 3}\right)\right]^{\sin\left[\frac{\pi}{2}\frac{\log(k^+/3)}{\log(25/3)}\right]} & \rightarrow \quad 3 \leq k^+ < 25 \\ \frac{1}{\kappa}\ln(0.49k^+ - 3) & \rightarrow \quad 25 \leq k^+ \end{cases} \tag{8}$$

in which, κ is the von-Karman constant ($\kappa = 0.42$).

2.2.3. Geometry and Boundary Conditions

The CFD simulations were carried out on the well-known container ship KCS modelled on the scale factor of 75, as used for [18]. Table 1 presents the particulars of the full-scale and model KCS adapted from Kim et al. [30] and [31].

Table 1. Kriso Container Ship (KCS) Full-scale and Model-scale principal characteristics.

Parameters		Full-scale	Model-scale
Scale factor	λ	1	75
Length between the perpendiculars	$L_{PP}\ (m)$	230	3.0667
Length of waterline	$L_{WL}\ (m)$	232.5	3.1
Beam at waterline	$B_{WL}\ (m)$	32.2	0.4293
Depth	$D\ (m)$	19.0	0.2533
Design draft	$T\ (m)$	10.8	0.144
Wetted surface area without rudder	$S\ (m^2)$	9424	1.6753
Displacement	$\nabla\ (m^3)$	52030	693.733
Block coefficient	C_B	0.6505	0.6505
Design speed	$V\ (kn, m/s)$	24	1.426
Froude number	F_n	0.26	0.6505
Reynolds number	R_n	$2.4 \cdot 10^9$	$3.7 \cdot 10^6$
Centre of gravity	$KG\ (m)$	7.28	0.0971
Metacentric height	$GM\ (m)$	0.6	0.008

Table 2 and Figure 3 depict the characteristics of the different hull roughness scenarios of the CFD simulations. It is of note that the total wetted surface area without rudder, S, of the KCS model used by Song et al. [18], and the actual one used in the present simulations ($S_{Total} = 1.7415\ m^2$) differs by (3.8%). In other words, the actual S_{Total} was used instead of the reference value, S, for consistency with the exact rough wetted surface areas of the heterogeneous scenarios read from the simulations. The effect of the difference between actual and reference values on the results has been considered negligible. Accordingly, the modified-wall function approach previously demonstrated by Song et al. [18] was assumed valid for this study.

Table 2. Test scenarios of the KCS model simulations in heterogeneous hull roughness conditions.

Roughness scenario	Rough wetted surface area $S_{Rough}\ (m^2)$	% Rough wetted surface area % S_{Rough} (%)
1. Bulbous Bow	0.0447	2.57
2. Fore Hull	0.3079	17.68
3. Midship	0.5137	29.49
4. Aft Hull	0.3331	19.12
5. Stern	0.1418	8.14
6. Flat Bottom	0.3992	22.91
Full Rough	1.7415	100

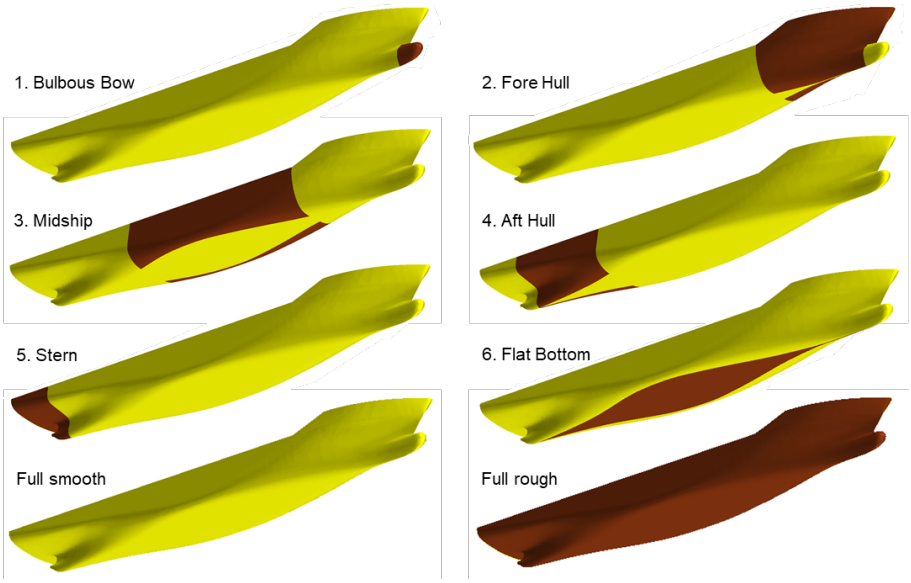

Figure 3. Test scenarios of the KCS model simulations in heterogeneous hull roughness conditions.

Figure 4 shows the computational domain, a towing tank with size chosen in accordance with ITTC recommendations [32] and similar studies [18], [22], [23]. A pressure outlet was chosen for the outlet boundary condition while a velocity inlet was applied for all the other surfaces of the domain (inlet, side walls, bottom and top). These boundary conditions simulated the deep water and infinite air conditions. Bottom, top and side walls of the tank were selected as slip-walls whilst for free-surface modelling, the no-slip wall type boundary condition was used on the hull surfaces. A symmetry boundary condition was applied on the vertical centre plane of the domain to shorten the computational time. No constraints were given to the model ship which was free to sink and trim.

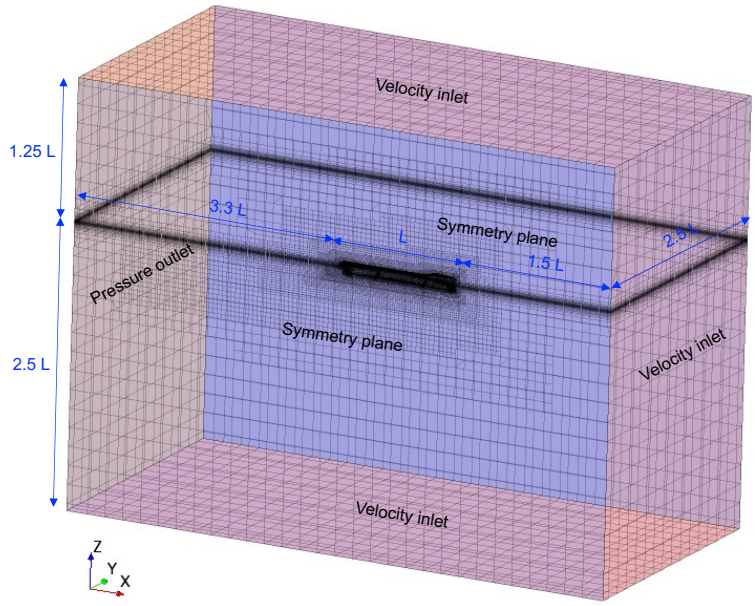

Figure 4. Computational domain and boundary conditions of the KCS model simulations.

2.2.4. Mesh Generation

Figure 5 shows the volume mesh of this CFD analysis. The built-in automated mesher of Star-CCM+ software was used to generate the trimmed hexahedral-dominant finite element mesh. Further near-wall mesh refinements were made applying mesh refinement on the critical regions such as the free surface, the bulbous bow, the stern, and the rough boundaries regions. For these simulations, the wall y^+ values were kept between 30 and 300 and higher than k^+ values, as recommended by Siemens [33]. All the simulations used the same mesh regardless of the hull roughness scenarios.

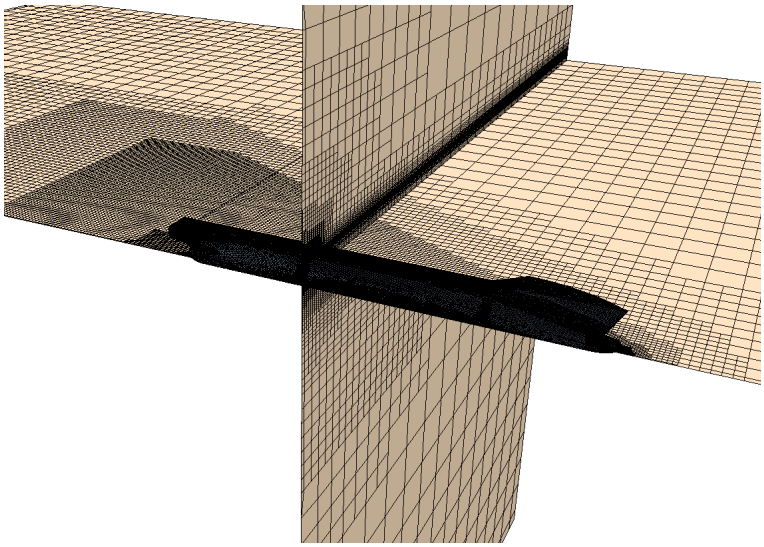

Figure 5. Volume mesh used for the KCS model simulations.

3. Results

3.1. Effect of Heterogeneous Roughness on Ship Resistance

Heterogeneous hull roughness affects the ship performances in a complicated, non-proportional way. Therefore, in this section the results of the towing tests conducted in CFD on the KCS model in heterogeneous hull roughness conditions are discussed and compared with the homogeneous fully smooth and fully rough cases. As reported above in Table 1, the simulations were carried out at a towing speed of $1.425\,m/s$, Froude number $Fn = 0.26$, and Reynolds number $Re_L = 3.74 \times 10^6$, which correspond to the full-scale design speed of KCS (24 knots) and $Re_L = 2.43 \times 10^9$. According to Froude's method, the total ship resistance coefficient, C_T, can be decomposed into the frictional resistance coefficient, C_F, and the residuary resistance coefficient, C_R, given by equation (9):

$$C_T = C_F + C_R \tag{9}$$

where the resistance coefficients C, are a function of the corresponding drag, R, the dynamic pressure, $1/2\,\rho V^2$, and the total wetted surface area of the ship hull, S. The total resistance coefficient, C_T, is defined as in equation (10):

$$C_T = \frac{R_T}{\frac{1}{2}\rho\, S\, V^2} \tag{10}$$

in which, ρ is the water density and V is the towing speed (i.e., the inlet velocity).

In Figure 6 and Table 3 are compared the resistance coefficients, total (C_T), frictional (C_F), residuary (C_R), and added (ΔC_F), of the KCS hull in heterogeneous roughness configurations. The added resistance coefficient, (or roughness allowance, ΔC_F), is the variation in the total resistance coefficient between the rough and smooth conditions. Different ΔC_F values were found across the fore-rough conditions (*Bulbous Bow*, *Fore Hull*), the midship-rough conditions (*Midship*, *Flat Bottom*), and the aft-rough conditions (*Aft Hull*, *Stern*) due to the different local increased hull roughness and hence locally increased skin friction of the hull. It would be expected that larger rough/smooth wetted surface area ratios would correspond to more significant resistance coefficients.

On the other hand, the present CFD simulations discredited this proportional assumption. For example, the *Bulbous Bow* case accounts for a smaller rough/smooth wetted surface area ratio than the Stern configuration, but its corresponding added resistance is greater. In fact, the *Bulbous Bow* rough/smooth wetted surface area ratio is 2.57% and the added resistance coefficient is $9.90 \cdot 10^{-5}$ while for the *Stern* case these parameters are 8.14% and $7.83 \cdot 10^{-5}$, respectively. In other words, the results of this study showed that the position of the selected area of the hull with increased surface roughness affects its impact on the ship hydrodynamics.

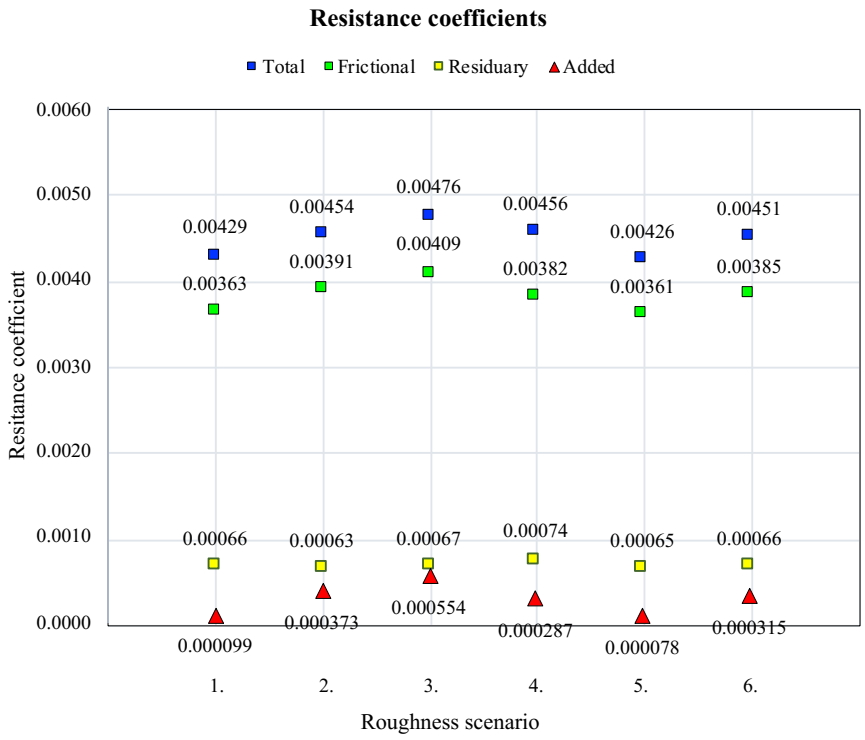

Figure 6. Resistance coefficients for the KCS model simulations in different hull roughness conditions.

Table 3. Resistance coefficients for the KCS model simulations in different hull roughness conditions.

Roughness scenario	Frictional C_F (-)	Residuary C_R (-)	Total C_T (-)	Added ΔC_F (-)
1. Bulbous Bow	$3.63 \cdot 10^{-3}$	$6.61 \cdot 10^{-4}$	$4.29 \cdot 10^{-3}$	$9.90 \cdot 10^{-5}$
2. Fore Hull	$3.91 \cdot 10^{-3}$	$6.32 \cdot 10^{-4}$	$4.54 \cdot 10^{-3}$	$3.73 \cdot 10^{-4}$
3. Midship	$4.09 \cdot 10^{-3}$	$6.73 \cdot 10^{-4}$	$4.76 \cdot 10^{-3}$	$5.54 \cdot 10^{-4}$
4. Aft Hull	$3.82 \cdot 10^{-3}$	$7.44 \cdot 10^{-4}$	$4.56 \cdot 10^{-3}$	$2.87 \cdot 10^{-4}$
5. Stern	$3.61 \cdot 10^{-3}$	$6.46 \cdot 10^{-4}$	$4.26 \cdot 10^{-3}$	$7.83 \cdot 10^{-5}$
6. Flat Bottom	$3.85 \cdot 10^{-3}$	$6.63 \cdot 10^{-4}$	$4.51 \cdot 10^{-3}$	$3.15 \cdot 10^{-4}$

Figure 7 and Table 4 highlight this non-proportional impact of increased roughness of the heterogeneous configurations. For the purpose of weighting the effect of increased heterogeneous hull roughness on added resistance a so-called "roughness impact factor", F_{RI}, has been defined as in equation (11):

$$F_{RI} = \frac{(\Delta C_F)_i / (S_{Rough})_i}{(\Delta C_F)_{Full\ Rough} / S_{Total}} \tag{11}$$

In which $(\Delta C_F)_i$ and $(S_{Rough})_i$ are, respectively, the added resistance and the rough wetted surface area of the i-th heterogeneous hull roughness case in exam. $(\Delta C_F)_{Full\ Rough}$ is the added resistance of the full rough hull surface condition, and S_{Total} is the total wetted surface area of the hull. Evidently, F_{RI} is unitary for the *Full Rough* scenario. For each case, the roughness impact factor, F_{RI}, correlates the added resistance coefficient to the rough wetted surface area.

It can be noted that while being the smallest area with increased hull roughness, the *Bulbous Bow* scenario has the most significant impact on ship resistance (impact factor of 2.49) of all the scenarios. The *Fore Hull* case has the second-largest impact (impact factor of 1.36). On the other hand, despite being the largest rough wetted surface area tested, the *Midship* configuration only gives an impact factor of 1.21. Similarly, the *Aft Hull*, *Stern* and *Flat Bottom* configurations showed the lowest impact factors of the heterogeneous scenarios tested. For these configurations, F_{RI} is lower than unity (0.97, 0.62, 0.89, respectively).

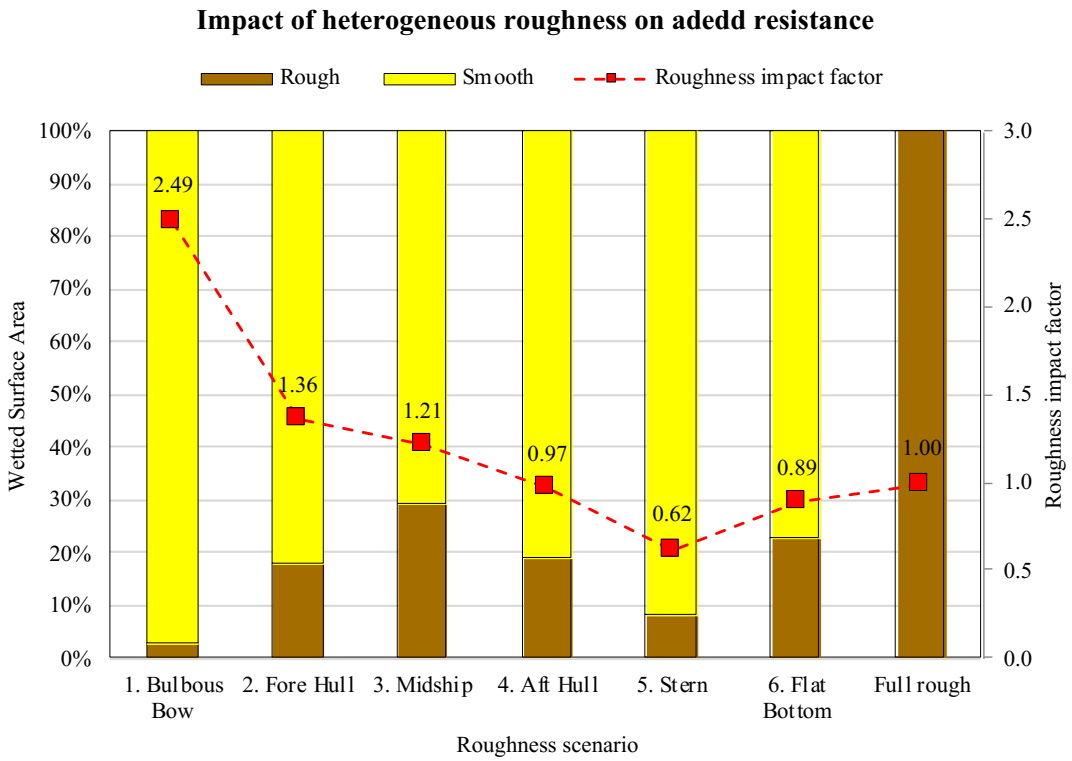

Figure 7. Roughness impact factors and wetted surface area ratios of the roughness scenario tested.

Table 4. Roughness impact factors and wetted surface area ratios of the roughness scenario tested.

Roughness scenario	Rough wetted surface area % S_R (%)	Added resistance coefficient ΔC_F (-)	Roughness impact factor F_{RI} (-)
1. Bulbous Bow	2.57	$1.98 \cdot 10^{-4}$	2.49
2. Fore Hull	17.68	$7.45 \cdot 10^{-4}$	1.36
3. Midship	29.49	$1.11 \cdot 10^{-3}$	1.21
4. Aft Hull	19.12	$5.74 \cdot 10^{-4}$	0.97
5. Stern	8.14	$1.57 \cdot 10^{-4}$	0.62
6. Flat Bottom	22.91	$6.30 \cdot 10^{-4}$	0.89
Full Rough	100	$3.10 \cdot 10^{-3}$	1

3.2. Rationale behind the Effect of Heterogeneous Roughness

The effect of hull roughness on ship resistance is closely related to the heterogeneous distribution of the increased roughness. Locally increased roughness affects the local skin friction coefficients, the Roughness Reynolds number values (k^+) and the boundary layer characteristics. A discussion and comparison of the local skin friction, the roughness Reynolds number, and the boundary layer of the KCS hull with heterogeneous hull roughness scenarios is presented.

Figure 8 compares the local skin friction coefficients, C_f, on the KCS hull in heterogeneous hull roughness conditions with the homogeneous full smooth and full rough cases (scalar field distribution on the hull surfaces limited to $C_f = 0.01$). The local skin friction coefficients, C_f, were obtained as in equation (12):

$$C_f = \frac{\tau_w}{\frac{1}{2}\rho V^2} \tag{12}$$

Where τ_w is the wall shear stress, ρ is the water density and V is the towing speed (i.e. the inlet velocity). The *Bulbous Bow* and *Fore Hull* roughness conditions in Figure 8-1 and Figure 8-2 show similar C_f distributions as that

of the *Full Rough* condition. The most significant increases in the local C_f values were observed for the upstream regions of the *Midship* configuration. In this case, the effect of the heterogeneous increase of hull roughness is dramatic, as shown in Figure 8-3. On the other hand, the *Aft Hull*, *Stern* and *Flat Bottom* scenarios (Figure 8-4,5,6) are less impactful on the skin friction coefficient distribution. Hence, C_f distributions are more similar to the *Full Smooth* homogeneous condition than to the *Full Rough*.

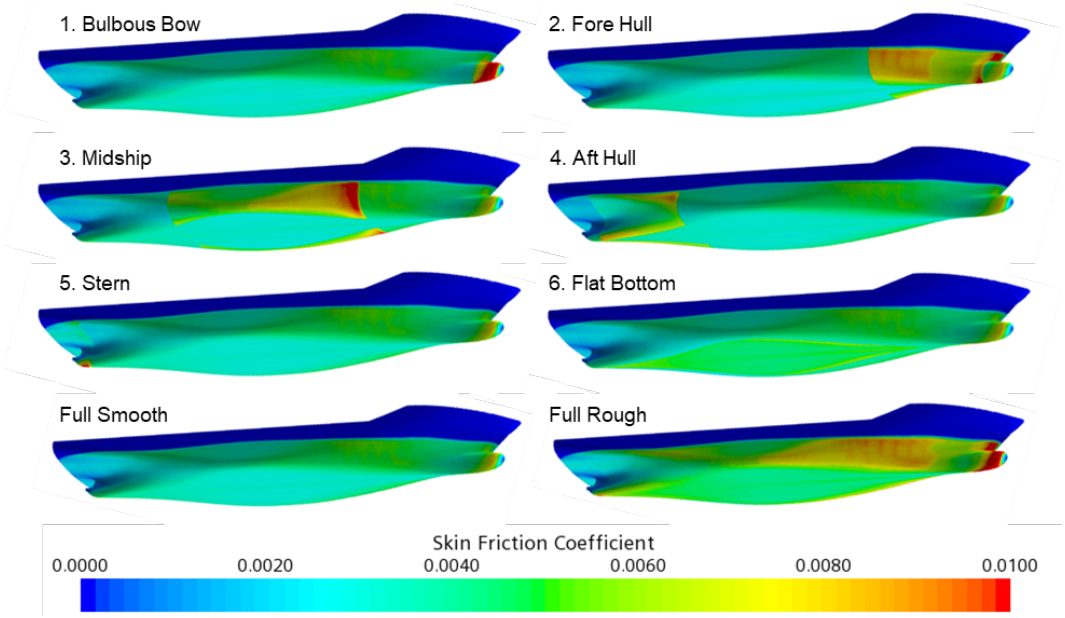

Figure 8. Skin friction coefficients (C_f) on the KCS hull in different hull roughness conditions at test speed ($Fn = 0.26$).

Figure 9 shows the distributions of the roughness Reynolds number, k^+, on the KCS hull in heterogeneous hull roughness conditions (scalar field distribution on the hull surfaces limited to $k^+ = 45.0$). The roughness Reynolds numbers were obtained as in equation (13):

$$k^+ = \frac{k\,\tau_w}{\nu} \tag{13}$$

Where k is the roughness height, τ_w is the wall shear stress, and ν is the kinematic viscosity. As shown in equation (8), the fully rough regime is reached when k^+value is higher than 25. The distributions of k^+ on the heterogeneous rough surfaces is similar to the bow regions of the homogeneous *Full Rough* case. Accordingly, the configurations 1, 2 and 3 show larger k^+ values than the scenarios 4, 5 and 6 due to the observed roughness effect.

The observation in Figure 8 and Figure 9 on the local skin friction coefficients, C_f, and the roughness Reynolds numbers, k^+, are strictly related to the previous findings shown in Table 3 and Table 4. It is well-known that the wall shear stress, τ_w, is more significant in the bow region of ship hulls due to the active transition behaviours, and it decreases as the flow develops along the hull. As the wall shear stress, τ_w, increases, it results in larger local skin friction coefficients and roughness Reynolds numbers in the bow regions. Accordingly, the roughness effect in the bow regions becomes more critical than in the stern regions.

Figure 10 shows the boundary layer on the KCS hull in heterogeneous hull roughness conditions. The boundary layer is represented by portions of transversal planes limited to the axial velocity, $V_x/V_{ship} = 0.9$. The roughness increase affects the boundary layer thickness around the hull in different ways, and the present results are in agreement with previous studies [6], [15], [20], [24], [34]. For the homogeneous cases, the *Full Rough* scenario shows a thicker boundary layer than the *Full Smooth* condition. shows the boundary layer on the KCS hull in heterogeneous hull roughness conditions. The boundary layer is represented by portions of transversal planes limited to the axial velocity, $V_x/V_{ship} = 0.9$. The roughness increase affects the boundary layer thickness around the hull in different ways, and the present results are in agreement with previous studies [6], [15], [20], [24], [34]. For the homogeneous cases, the *Full Rough* scenario shows a thicker boundary layer than the *Full Smooth* condition.

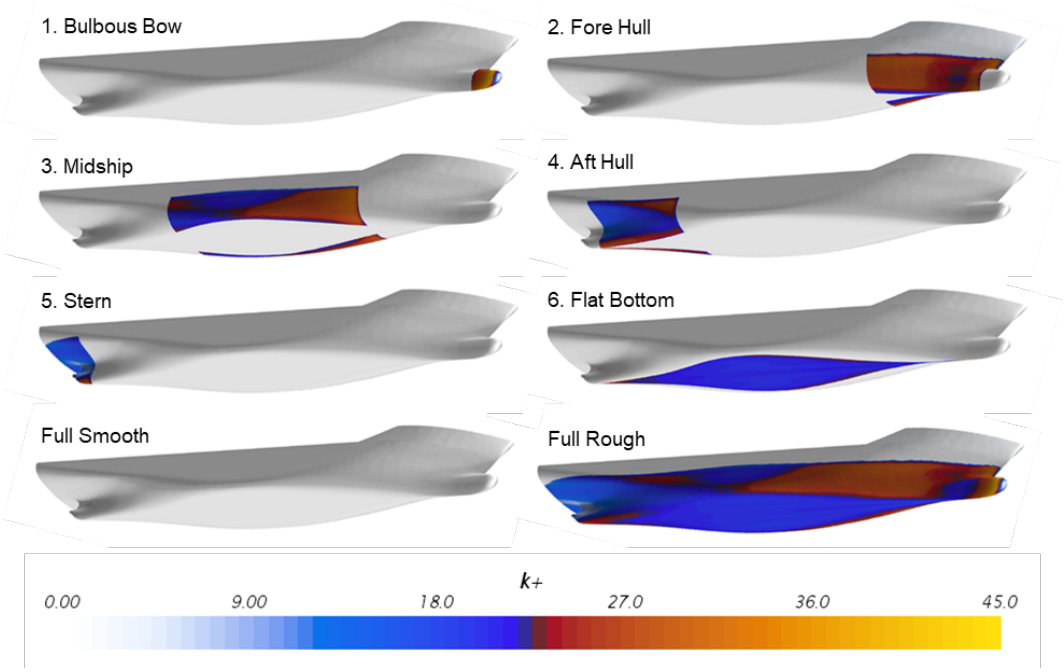

Figure 9. Roughness Reynolds number (k^+) distribution on the KCS hull in different hull rougness condtions at test speed ($Fn = 0.26$).

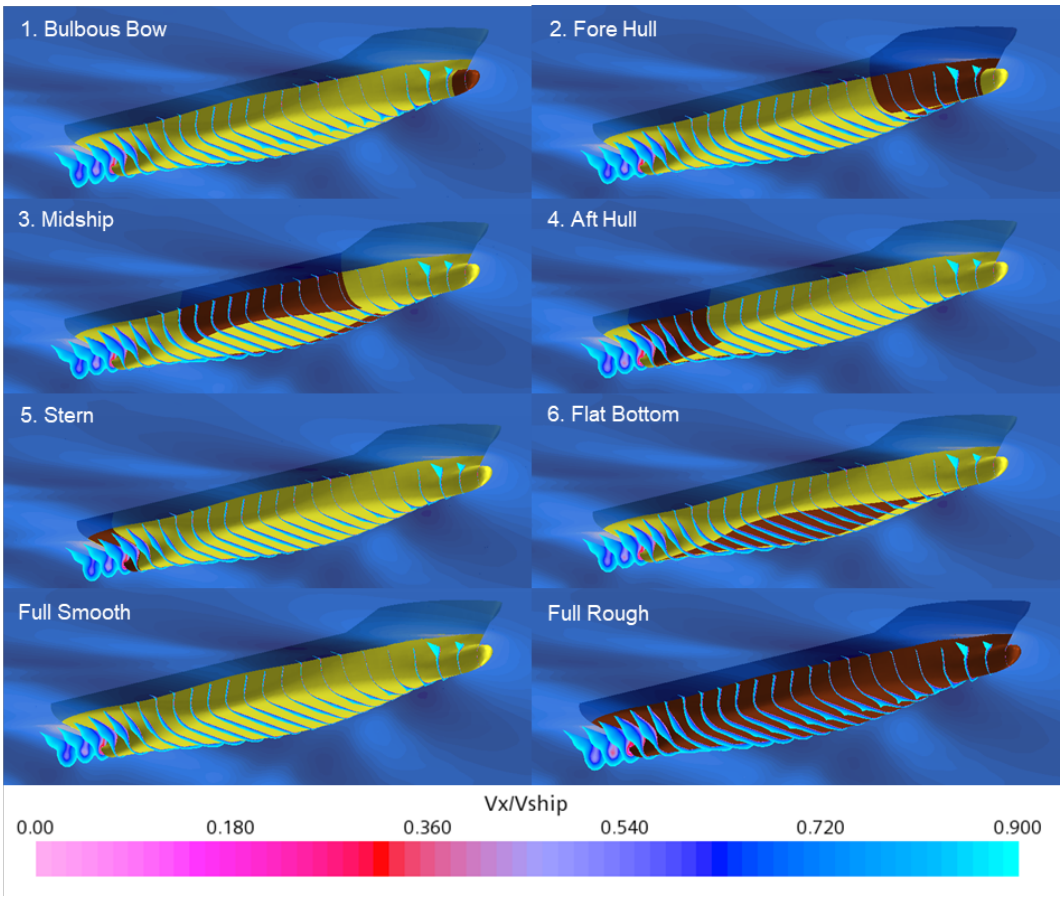

Figure 10. Boundary layer on the KCS hull in different hull roughness conditions at test speed ($Fn = 0.26$).

Furthermore, the differences between *Full Rough* and *Full Smooth* configurations become apparent in the bow regions where the increased roughness causes a thicker boundary layer, peak-shaped on the symmetry plane. Interestingly, the boundary layer of the *Bulbous Bow* case (Figure 10-1) is similar to that of the *Full Rough* condition. While, despite a similar thickness of the boundary layer, the *Fore Hull* case shows a much less evident

pointy shape (Figure 10-2). On the other hand, as shown in Figure 10-3,4,5,6, the boundary layer thickness around the hull showed almost no differences compared to that of the *Full Smooth* case.

It could be assumed that a rough bulbous bow region is responsible for the sharp characteristic of the boundary layer, culminating on the symmetry plane. Perhaps the rationale behind the significant roughness impact factor of the bulbous bow region lies in its extensive influence on the boundary layer characteristics.

4. Conclusions

An investigation on the effect of heterogeneous hull roughness on ship resistance components and characteristics of the flow around the hull was carried out. URANS-based CFD simulations were carried out on the well-known KCS hull model in different hull roughness conditions. A modified wall-function approach was adopted to implement the roughness characteristics of the surfaces in the CFD model. The different scenarios studied were intended to assess the roughness effect of different parts of the hull on the ship hydrodynamics. The observations on the effects of heterogeneous hull roughness were correlated with the rough wetted surface areas, the distributions of the local skin friction coefficients, the roughness Reynolds number values, and the boundary layer characteristics. Furthermore, comparisons with the homogeneous full rough-smooth cases were presented.

The CFD towing tests showed that the rough regions tested (namely *Bulbous Bow*, *Fore Hull*, *Midship*, *Aft Hull*, *Stern* and *Flat Bottom*) had a different impact on the ship resistance due to their position on the hull. A *roughness impact factor*, F_{RI}, was defined to predict this impact. The evidence confirmed that the added resistance observed for the fore-rough regions is proportionately greater than for the aft-rough regions. In other words, the roughness conditions of the fore regions proportionally affect the ship hydrodynamics more than the aft regions. The present study supported similar observations of other researchers [6], [15], [20], [24], [34].

Interestingly, the present findings showed that the rough *Bulbous Bow* condition presents the greater roughness impact factor ($F_{RI} = 2.49$), despite the smaller percentage of rough wetted surface area. Thus, the rough bulbous bow scenario led to the proportionately greater added resistance than other rough regions of the hull. On the other hand, the rough *Stern* case present the smaller roughness impact factor ($F_{RI} = 0.62$), confirming that the surface conditions of the aft regions of the hull have a minor impact on ship resistance.

The numerical investigation presented in this study provides valuable results from a practical point of view. The roughness impact of different hull regions has been investigated, adopting a widely accepted and validated CFD approach. Naval architects, ship owners, and operators could benefit from this study's insight and target limited-time maintenance on the fore-hull regions affecting the ship resistance the most. When complete maintenance on the entire hull is not feasible, it could be worth cleaning the fore hull parts first.

Future studies could focus on comparing the numerical results presented in this study with measurements obtained from tow testing CFD simulations could be conducted to investigate further heterogeneous hull roughness configurations and their effect on ship resistance.

5. Acknowledgements

The authors acknowledge the support of the EU funded H2020 project, VENTuRE (grant no. 856887, https://h2020venture.eu/), and of the ARCHIE-WeSt High-Performance Computer (www.archie-west.ac.uk).

6. References

[1] R. L. Townsin, "The Ship Hull Fouling Penalty," *Biofouling*, vol. 19, no. sup1, pp. 9–15, 2003.

[2] T. Tezdogan and Y. K. Demirel, "An overview of marine corrosion protection with a focus on cathodic protection and coatings," *Brodogradnja*, vol. 65, no. 2, pp. 49–59, 2014.

[3] Y. K. Demirel, "Modelling the Roughness Effects of Marine Coatings and Biofouling on Ship Frictional Resistance," University of Strathclyde, 2015.

[4] M. Candries, "Drag, Boundary-layer and roughness characteristics of marine surfaces coated with antifoulings," University of Newcastle, 2001.

[5] M. P. Schultz, "Frictional resistance of antifouling coating systems," *J. Fluids Eng. Trans. ASME*, vol. 126, no. 6, pp. 1039–1047, 2004.

[6] M. P. Schultz and K. A. Flack, "Outer layer similarity in fully rough turbulent boundary layers," *Exp. Fluids*, vol. 38, no. 3, pp. 328–340, Mar. 2005.

[7] T. Shapiro, "The Effect of Surface Roughness on Hydrodynamic Drag and Turbulence," US Naval Academy Annapolis, 2004.

[8] M. P. Schultz, "The relationship between frictional resistance and roughness for surfaces smoothed by sanding," *J. Fluids Eng. Trans. ASME*, vol. 124, no. 2, pp. 492–499, Jun. 2002.

[9] K. A. Flack and M. P. Schultz, "Review of hydraulic roughness scales in the fully rough regime," *Journal of Fluids Engineering, Transactions of the ASME*, vol. 132, no. 4. pp. 0412031–04120310, 2010.

[10] M. P. Schultz, "Effects of coating roughness and biofouling on ship resistance and powering," *Biofouling*, vol. 23, no. 5, pp. 331–341, Oct. 2007.

[11] P. S. Granville, "Similarity-law characterization methods for arbitrary hydrodynamic roughnesses," Bethesda: Rockville, MD, USA, Feb. 1978.

[12] P. S. Granville, "The Frictional Resistance and Turbulent Boundary Layer of Rough Surfaces," *J. Sh. Res.*, vol. 2, no. 04, pp. 52–74, Dec. 1958.

[13] D. Oliveira, A. I. Larsson, and L. Granhag, "Effect of ship hull form on the resistance penalty from biofouling," *Biofouling*, vol. 34, no. 3, pp. 262–272, Mar. 2018.

[14] M. Atlar *et al.*, "A Rational Approach to Predicting the Effect of Fouling Control Systems on 'In-Service' Ship Performance," in *GMO J. Ship Mar. Technol.*, 2018, p. 213.

[15] Y. K. Demirel, D. Uzun, Y. Zhang, H.-C. Fang, A. H. Day, and O. Turan, "Effect of barnacle fouling on ship resistance and powering," *Biofouling*, vol. 33, no. 10, pp. 819–834, Nov. 2017.

[16] F. Stern *et al.*, "Recent progress in CFD for naval architecture and ocean engineering," *Journal of Hydrodynamics*, vol. 27, no. 1. pp. 1–23, 2015.

[17] J. Wang and D. Wan, "Application Progress of Computational Fluid Dynamic Techniques for Complex Viscous Flows in Ship and Ocean Engineering," *J. Mar. Sci. Appl.*, vol. 19, no. 1, 2020.

[18] S. Song, Y. K. Demirel, M. Atlar, S. Dai, S. Day, and O. Turan, "Validation of the CFD approach for modelling roughness effect on ship resistance," *Ocean Eng.*, vol. 200, no. February, p. 107029, 2020.

[19] Y. K. Demirel, O. Turan, and A. Incecik, "Predicting the effect of biofouling on ship resistance using CFD," *Appl. Ocean Res.*, vol. 62, pp. 100–118, Jan. 2017.

[20] S. Song, Y. K. Demirel, and M. Atlar, "An investigation into the effect of biofouling on the ship hydrodynamic characteristics using CFD," *Ocean Eng.*, vol. 175, no. January, pp. 122–137, 2019.

[21] S. Song, Y. K. Demirel, C. De Marco Muscat-Fenech, T. Tezdogan, and M. Atlar, "Fouling effect on the resistance of different ship types," *Ocean Eng.*, vol. 216, p. 107736, Nov. 2020.

[22] S. Song *et al.*, "Experimental investigation on the effect of heterogeneous hull roughness on ship resistance," *Ocean Eng.*, vol. 223, Mar. 2021.

[23] S. Song, Y. K. Demirel, C. De Marco Muscat-Fenech, T. Sant, and D. Villa, "Investigating the Effect of Heterogeneous Hull Roughness on Ship Resistance Investigating the Effect of Heterogeneous Hull Roughness on Ship Resistance Using CFD," *J. Mar. Sci. Eng.*, vol. 9, no. 202, 2021.

[24] S. Song, S. Dai, Y. K. Demirel, M. Atlar, S. Day, and O. Turan, "Experimental and Theoretical Study of the Effect of Hull Roughness on Ship Resistance," *J. Sh. Res.*, vol. 65, no. 1, pp. 62–71, 2021.

[25] A. Vargas, H. Shan, and E. Holm, "Using CFD to Predict Ship Resistance due to Biofouling, and Plan Hull Maintenance," in *4th Hull Performance & Insight Conference (HullPIC'19)*, 2019, pp. 242–254.

[26] A. Östman, K. Koushan, and L. Savio, "Study on Additional Ship Resistance due to Roughness using CFD," *J. Sh. Mar. Technol. J.*, vol. 216, Dec. 2019.

[27] "KCS Geometry and Conditions," *SIMMAN 2008, FORCE Technology*, 2008. [Online]. Available:

http://www.simman2008.dk/KCS/kcs_geometry.htm. [Accessed: 07-Jun-2021].

[28] J. H. Ferziger, M. Perić, and R. L. Street, *Computational Methods for Fluid Dynamics*. Springer International Publishing, 2020.

[29] F. R. Menter, "Two-Equation Eddy-Viscosity Turbulence Models for Engineering Applications," *AIA A J.*, vol. 32, no. 8, 1994.

[30] W. J. Kim, S. H. Van, and D. H. Kim, "Measurement of flows around modern commercial ship models," *Exp. Fluids*, vol. 31, no. 5, pp. 567–578, Nov. 2001.

[31] L. Larsson, F. Stern, and M. Visonneau, "CFD in ship hydrodynamics - Results of the Gothenburg 2010 workshop," in *Computational Methods in Applied Sciences*, 2013, vol. 29, pp. 237–259.

[32] ITTC, "ITTC-Recommended Procedures and Guidelines Practical Guidelines for Ship CFD Applications," 2011.

[33] Siemens, "STAR-CCM+, User Guide. Version 15.06." 2020.

[34] M. P. Schultz and K. A. Flack, "The rough-wall turbulent boundary layer from the hydraulically smooth to the fully rough regime," *J. Fluid Mech.*, vol. 580, pp. 381–405, Jun. 2007.